EUROPEAN
JOURNAL OF
MECHANICS
A/SOLIDS

Modification of the Gurson Model for shear failure

K. Nahshon, J.W. Hutchinson *

School of Engineering and Applied Sciences, Harvard University, Cambridge, MA 02138, USA

Abstract

Recent experimental evidence points to limitations in characterizing the critical strain in ductile fracture solely on the basis of stress triaxiality. A second measure of stress state, such as the Lode parameter, is required to discriminate between axisymmetric and shear-dominated stress states. This is brought into the sharpest relief by the fact that many structural metals have a fracture strain in shear, at zero stress triaxiality, that can be well below fracture strains under axisymmetric stressing at significantly higher triaxiality. Moreover, recent theoretical studies of void growth reveal that triaxiality alone is insufficient to characterize important growth and coalescence features. As currently formulated, the Gurson Model of metal plasticity predicts no damage change with strain under zero mean stress, except when voids are nucleated. Consequently, the model excludes shear softening due to void distortion and inter-void linking. As it stands, the model effectively excludes the possibility of shear localization and fracture under conditions of low triaxiality if void nucleation is not invoked. In this paper, an extension of the Gurson model is proposed that incorporates damage growth under low triaxiality straining for shear-dominated states. The extension retains the isotropy of the original Gurson Model by making use of the third invariant of stress to distinguish shear dominated states. The importance of the extension is illustrated by a study of shear localization over the complete range of applied stress states, clarifying recently reported experimental trends. The extension opens the possibility for computational fracture approaches based on the Gurson Model to be extended to shear-dominated failures such as projectile penetration and shear-off phenomena under impulsive loadings.
© 2007 Elsevier Masson SAS. All rights reserved.

Keywords: Plasticity; Void growth; Shear localization; Shear fracture; Gurson Model; Lode parameter

1. Introduction

The role of stress triaxiality (defined as σ_m/σ_e with mean stress $\sigma_m = \sigma_{kk}/3$ and effective stress $\sigma_e = \sqrt{3 s_{ij} s_{ij}/2}$ with s_{ij} as the stress deviator) in ductile fracture of ductile structural metals is well known. Much experimental data shows a monotonic decrease in effective plastic strain at fracture when plotted against stress triaxiality, although most of this data was acquired under axisymmetric stress states (Hancock and Mackenzie, 1976; Le Roy et al., 1981; Johnson-Cook, 1985). Mean stress has little or no influence on overall plastic deformation in the absence of damage, but it has a dramatic effect on the ductile fracture mechanism, particularly on void growth and coalescence. Although the Gurson Model (Gurson, 1977) of dilatational plasticity is phenomenological, its dependence on mean stress is formulated consistent with the mechanics of void growth under axisymmetric stress states (McClintock, 1968; Rice

---

* Corresponding author.
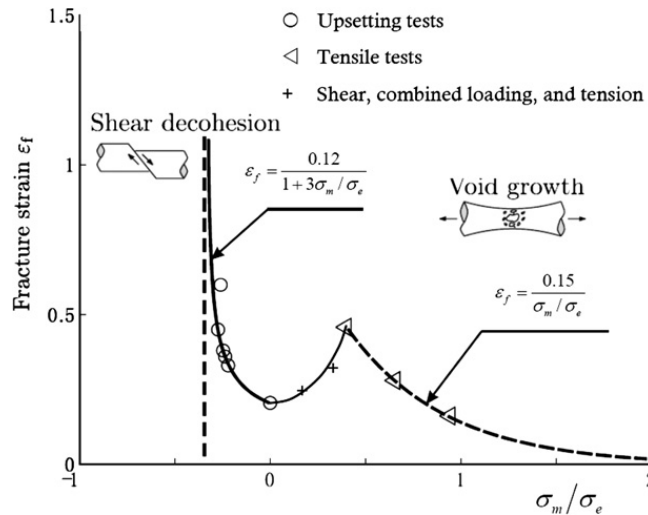*E-mail address:* jhutchin@fas.harvard.edu (J.W. Hutchinson).

Fig. 1. Effective strain at fracture for Al 2024-T351. Data from Bao and Wierzbicki (2004) with figure adapted from Teng and Wierzbicki (2006).

and Tracey, 1969). The success of the model in a wide array of applications involving failure phenomena such as shear localization, crack initiation and crack growth (e.g. Rousselier, 1987; Howard et al., 1994; Xia et al., 1995; Gullerud et al., 2000) attests to the fidelity of its mechanistic underpinnings. The article by Tvergaard (1990) provides a complete presentation of the model and some of its applications, along with proposals made subsequent to the original Gurson Model to improve its accuracy.

One important limitation of the Gurson Model which has become apparent in recent years is its inapplicability to localization and fracture for low triaxiality, shear-dominated deformations such as plugging failure due to projectile penetration, cropping and dynamic shear-off. The Gurson Model identifies a single damage parameter, f, as the average, or effective, void volume fraction. According to the model, an increase in f due to the incremental grow of voids requires a positive mean stress. Thus, for example, in shearing deformations under zero mean stress, the model predicts no increase in damage if continuous void nucleation is not invoked. As a consequence, no damage induced softening takes place under shear in materials with inherent strain hardening capacity, and neither localization nor material failure occurs.

The derivation of yield function of the Gurson Model (Gurson, 1977) employed spherical voids and based the void growth mechanics on axisymmetric stress states, following the approach of Rice and Tracey (1969). It has long been appreciated that the effect of penny-shaped crack-like voids aligned perpendicular to the principal stress direction can be captured approximately by the model by regarding the voids as nominally spherical with a volume fraction, f, tied not to the actual volume fraction of the cracks but to the radius and spacing of the cracks. The Gurson Model has been extended to include void shape dependences by a number of authors including Gologanu et al. (1995) and Pardoen and Hutchinson (2000) who made use of basic mechanics solutions of Leblond et al. (1995). However, these extensions are also mainly based on solutions for voids subject to axisymmetric stressing and they do not address the issue of damage induced softening in shear-dominated deformations.

Experimental evidence for the susceptibility to shear fracture under low or even negative triaxiality has been presented by numerous authors. McClintock (1971) documented important cases where ductility is terminated by shear localization and shear cracking, and he provided theoretical insights using the slip line field theory of perfect plasticity. While Johnson and Cook (1985) are usually cited for emphasizing the trend of decreasing ductility with increasing triaxiality, they also report a fracture strain for 4340 steel at zero mean stress (obtained from a torsion test) that is well below fracture strains for this material at significantly higher mean stresses obtained under axisymmetric conditions from notched tension specimens. More recently, Bao and Wierzbicki (2004) have presented data that emphasizes that the relation between the effective plastic strain at fracture and mean stress is not generally monotonic, as illustrated by their plot for Al 2024-T351 shown here in Fig. 1. The two branches of the curve through the data correspond to distinct classes of stress states for which triaxiality alone is obviously not an adequate discriminate. For triaxialities above 0.4 the fracture data in Fig. 1 was obtained using circumferentially notched, axisymmetric tensile specimens such that fracture is initiated under stress states that are nominally axisymmetric. At triaxialities that are zero and below, upsetting specimens were used with shear cracks initiating at the specimen surface where a biaxial stress state

exists with one component tensile and the other compressive. When the mean stress is zero, the stress state is pure shear and a shear crack is observed to form aligned with the plane of maximum shear stress. Two data points at intermediate low triaxialities were obtained using tension-shear specimens.

Most recently, Barsoum and Faleskog (2007a) tested circumferentially notched tubes of both mid-strength and high strength Weldox steels in combined tension and torsion with the specific purpose of delineating the roles of stress triaxiality and a second stress measure, the Lode parameter, capable of discriminating between axisymmetric and plane strain stress states. They also reported susceptibility to fracture under low triaxiality shearing.

Theoretical studies have been conducted in parallel by Barsoum and Faleskog (2007b) and Gao and Kim (2006) employing cell model computations for three dimensional arrays of initially spherical voids subject to a wide range of overall stress states. These authors have shown that the triaxiality measure by itself is insufficient to characterize void growth rates and other aspects of void behavior relevant to softening and localization.

Knowledge of the underlying mechanisms of softening, localization and fracture in shear is more qualitative than quantitative, but relevant experimental and theoretical work exists in the literature. Continuous nucleation of voids by itself can counteract inherent material strain hardening capacity to result in softening. The emphasis here is on mechanisms such as void distortion and inter-void interaction in shear that give rise to softening and localization. McClintock (1971) and Teirlinck et al. (1988) discuss specific examples of shear fracture and identify void-sheet formation as the underlying mechanism wherein it is supposed that under shearing voids increase their effective collective cross-sectional area parallel to the localization band without an accompanying increasing in void volume. Localization in shear in micro bands linking voids is evident in the model voided materials tested by Weck et al. (2006). Simulation of softening and localization in shear is not straightforward. The cell model studies of Barsoum and Faleskog (2007b) for overall shear deformation with zero mean stress display shear-weakening, but not softening. Instead, the authors employ attainment of a critical strain in the ligaments between voids as their criterion for shear failure. Anderson et al. (1990) analyzed the shear fracture localization mechanism at zero mean stress by considering the detailed interaction between flat voids modeled as micro-cracks in a void-sheet. They found that softening and, therefore, localization are expected solely due to deformation and rotation of the voids.

2. Stress measures for dilatational plasticity

In this section an additional stress measure that distinguishes between axisymmetric and shear stress states is introduced to extend the Gurson Model. Isotropy of the model will be retained. The Gurson Model employs the mean stress, $\sigma_m = \sigma_{kk}/3$, and the effective stress, $\sigma_e \equiv \sqrt{3J_2} = \sqrt{3s_{ij}s_{ij}/2}$, where $s_{ij} = \sigma_{ij} - 1/3\sigma_{kk}\delta_{ij}$ is the stress deviator. A third invariant of stress is

$$J_3 = \det(\mathbf{s}) = \frac{1}{3}s_{ij}s_{ik}s_{jk} = (\sigma_{\mathrm{I}} - \sigma_m)(\sigma_{\mathrm{II}} - \sigma_m)(\sigma_{\mathrm{III}} - \sigma_m) \tag{1}$$

where the expression on the right is in terms of the principal stresses, which in the sequel are assumed to be ordered as $\sigma_{\mathrm{I}} \geqslant \sigma_{\mathrm{II}} \geqslant \sigma_{\mathrm{III}}$. Any *axisymmetric stress state* satisfies

$$\sigma_{\mathrm{I}} \geqslant \sigma_{\mathrm{II}} = \sigma_{\mathrm{III}} \quad \text{or} \quad \sigma_{\mathrm{I}} = \sigma_{\mathrm{II}} \geqslant \sigma_{\mathrm{III}}, \tag{2}$$

and it is readily shown that $J_3 = \pm 2(\sigma_{\mathrm{I}} - \sigma_{\mathrm{III}})^3/27 = \pm 2\sigma_e^3/27$. Any state which is the sum of *a pure shear stress plus a hydrostatic contribution*,

$$\sigma_{\mathrm{I}} = \tau + \sigma_m, \quad \sigma_{\mathrm{II}} = \sigma_m, \quad \sigma_{\mathrm{III}} = -\tau + \sigma_m (\tau > 0), \tag{3}$$

has $J_3 = 0$ by (1). The measure

$$\omega(\boldsymbol{\sigma}) = 1 - \left(\frac{27J_3}{2\sigma_e^3}\right)^2 \tag{4}$$

lies in the range, $0 \leqslant \omega \leqslant 1$, with $\omega = 0$ for all axisymmetric stress states and $\omega = 1$ for all states comprised of a pure shear stress plus a hydrostatic contribution, as illustrated by the plot of ω as function of $\sigma_{\mathrm{II}}/\sigma_{\mathrm{I}}$ for $\sigma_{\mathrm{III}} = 0$ given in Fig. 2.

The Lode parameter

$$L = \frac{2\sigma_{\mathrm{II}} - \sigma_{\mathrm{I}} - \sigma_{\mathrm{III}}}{\sigma_{\mathrm{I}} - \sigma_{\mathrm{III}}} = \frac{3(\sigma_{\mathrm{II}} - \sigma_m)}{\sigma_{\mathrm{I}} - \sigma_{\mathrm{III}}} \tag{5}$$

Fig. 2. ω vs $\sigma_{\mathrm{II}}/\sigma_{\mathrm{I}}$ for plane stress ($\sigma_{\mathrm{III}} = 0$).

Fig. 3. Lines of constant ω and L in principal-stress space.

has also been used as a third measure of the stress state in isotropic plasticity, and more recently it has been employed by Xue (2007a, 2007b) in studying Bao and Wierzbicki's (2004) data and by Barsoum and Faleskog (2007a) in presenting their own data. Note that L vanishes if $\sigma_{\mathrm{II}} = \sigma_m$, corresponding to states of pure shear stress plus a hydrostatic component in (3). Fig. 2 includes the variation of L under plane stress conditions.

The map of stress states in Fig. 3 is useful in understanding the role of the two measures. Attention is limited to states with at least one tensile principal stress component such that $\sigma_{\mathrm{I}} > 0$. The full range of states lies within the angular region ABD in Fig. 3. All axisymmetric stress states (2) lie on either AB or AD. The line AC constitutes all stress states comprised of a pure shear stress plus a hydrostatic contribution. As noted in Fig. 3, ω varies from 0 on AB peaking at 1 on AC and falling back to 0 on AD, while L increases monotonically from -1 to 1 across the same lines. As the existing versions of the Gurson model have been formulated and calibrated based on the mechanics of void growth under axisymmetric stress states, the modification introduced in this paper will not alter the model for these states. Instead, the model will be modified for states centered on a pure shear stress plus a hydrostatic contribution as

in (3). Specifically, we will include a contribution to void damage growth depending on ω that does not vanish when $\sigma_m = 0$.

3. Modified Gurson Model

The yield surface of the Gurson Model, including the fitting parameters, q_1, q_2 and q_3, proposed by Tvergaard (1981, 1982), is given in terms of the effective and mean stress measures by

$$F(\sigma_e, \sigma_m, f) = \left(\frac{\sigma_e}{\sigma_M}\right)^2 + 2q_1 f \cosh\left(\frac{3q_2}{2}\frac{\sigma_m}{\sigma_M}\right) - (1 + q_3 f^2). \tag{6}$$

The current state is characterized by f, the void volume fraction, and σ_M, the effective stress governing flow of the undamaged matrix material containing the voids. Throughout this paper, all quantities not labeled with the subscript M represent overall quantities associated with the bulk material. The yield function (6) is retained in the modified model.

Normality implies that the plastic strain rate, D_{ij}^P, is given by

$$D_{ij}^P = \frac{1}{h} P_{ij} P_{kl} \dot{\sigma}_{kl} \tag{7}$$

where

$$P_{ij} = \frac{\partial F}{\partial \sigma_{ij}} = \frac{3s_{ij}}{\sigma_M^2} + \frac{f q_1 q_2}{\sigma_M} \sinh\left(\frac{3q_2\sigma_m}{2\sigma_M}\right)\delta_{ij}. \tag{8}$$

Subsequently, $\dot{\sigma}_{ij}$ will be identified with the Jaumann rate of stress. The hardening modulus, h, will be identified below. If $\sigma_m = 0$, $P_{kk} = 0$ and the rate of plastic volume change vanishes, i.e. $D_{kk}^P = 0$; this feature persists in the modified version. In the absence of nucleation, existing versions of Gurson Model assume

$$\dot{f} = (1 - f)D_{kk}^P. \tag{9}$$

Because the void volume fraction is the damage parameter in the Gurson Model, the model implies no damage evolution in deformations involving zero mean stress, as emphasized in the introduction. This appears to be realistic when the stress states are axisymmetric, as established by computational models of void growth, but it is not realistic for states of pure shear stress, as discussed in the Introduction.

Motivated by the issues outlined in the Introduction, we modify (9) to include a contribution to the damage growth rate, $\dot{f}$, for states of pure shear stress in a manner which leaves the relation unaltered for axisymmetric stress states. The modification rests on the notion discussed in the Introduction that the volume of voids undergoing shear may not increase, but void deformation and reorientation contribute to softening and constitute an effective increase in damage. Thus, in the modification, f is no longer directly tied to the plastic volume change. Instead, it must be regarded either as an effective void volume fraction or simply as the damage parameter, as is often the case when the Gurson Model has been applied to materials with voids with distinctly non-spherical shapes. The modification, while phenomenological, is nevertheless formulated to be consistent with the mechanism of void softening in shear. Specifically, it is proposed that (9) be augmented according to

$$\dot{f} = (1 - f)D_{kk}^p + k_\omega f \omega(\boldsymbol{\sigma}) \frac{s_{ij} D_{ij}^p}{\sigma_e} \tag{10}$$

where $\omega(\boldsymbol{\sigma})$ is defined in (4). The additional contribution to $\dot{f}$ scales with $k_\omega f \omega D^P$, such that in a state of pure shear stress, $\dot{f} \sim k_\omega f \dot{\gamma}^P$, where $\dot{\gamma}^P$ is the plastic shear strain increment. The numerical constant, k_ω, sets the magnitude of the damage growth rate in pure shear states, as will be detailed in the next section; it is the single new parameter that enters the modified model. The additional contribution to $\dot{f}$ is linear in f under the assumption that the effective void volume fraction is small. In principle, any monotonic dependence on ω that vanishes at $\omega = 0$ and is maximum at $\omega = 1$, could be employed in (9), but the simplest linear dependence has been used in the absence of further mechanistic calibration. It can also be noted that $s_{ij} D_{ij}^P$ in (10) could be replaced by $\sigma_{ij} D_{ij}^P$ with minor effect.

The remaining equations governing increments in the modified model are now listed. Void nucleation is not included but it can readily be incorporated (e.g. Needleman and Rice, 1978; Chu and Needleman, 1980; Tvergaard, 1990). The consistency condition for continued plastic loading,

$$\dot{F} = \frac{\partial F}{\partial \sigma_{ij}} \dot{\sigma}_{ij} + \frac{\partial F}{\partial \sigma_M} \dot{\sigma}_M + \frac{\partial F}{\partial f} \dot{f} = 0, \tag{11}$$

provides the expression for the hardening modulus,

$$h = -\left[\left((1-f) P_{kk} + k_\omega \frac{f\omega}{\sigma_e} P_{ij} s_{ij} \right) \frac{\partial F}{\partial f} + \frac{h_M}{(1-f)\sigma_M} \frac{\partial F}{\partial \sigma_M} P_{ij} \sigma_{ij} \right]. \tag{12}$$

Here,

$$\frac{\partial F}{\partial \sigma_M} = -\frac{2\sigma_e^2}{\sigma_M^3} + \frac{3q_1 q_2 f \sigma_m}{\sigma_M^2} \sinh\left(\frac{3q_2 \sigma_m}{2\sigma_M} \right), \tag{13}$$

$$\frac{\partial F}{\partial f} = 2q_1 \cosh\left(\frac{3q_2 \sigma_m}{2\sigma_M} \right) - 2q_3 f \tag{14}$$

and h_M is the modulus of the matrix material defined in terms of the logarithmic plastic strain and true stress in uniaxial tension as

$$\frac{1}{h_M} = \frac{d\varepsilon_M^P}{d\sigma_M}. \tag{15}$$

The matrix material (i.e. the undamaged material with $f = 0$) is defined by its Young's modulus, E, Poisson's ratio, ν, and relation between logarithmic plastic strain and true stress in uniaxial tension, $\varepsilon_M^P(\sigma_M)$, also considered as the relation between effective plastic strain and effective stress. These are inputs to the modified Gurson Model along with the new parameter k_ω and initial value of f. The limit of the modified Gurson Model when $f \to 0$ is classical isotropic plasticity theory based on the Mises yield surface. As in the original model, plastic work in the matrix is equated to macroscopic plastic work according to

$$(1-f)\sigma_M \dot{\varepsilon}_M^P = \sigma_{ij} D_{ij}^P, \tag{16}$$

such that increments in matrix flow stress can be computed from

$$\dot{\sigma}_M = \frac{h_M \sigma_{ij} D_{ij}^P}{(1-f)\sigma_M}. \tag{17}$$

The final step is to identify the stress-rate for finite strain applications and to combine the elastic and plastic strain increments. The stress increments, $\dot{\sigma}_{ij}$, in the above development are identified with objective Jaumann increments, $\hat{\sigma}_{ij}$, whose Cartesian components coincide with true stress increments for straining in axes parallel to principal stress axes. Void damage diminishes the overall elastic moduli of the material. However, this is a small effect compared to void influence on plastic behavior and the effect on elasticity is neglected, as usually done in this type of model. Isotropic elastic behavior is assumed. Combining elastic strain rates, D_{ij}^e, and plastic strain rates from (7) gives the total strain rate as

$$D_{ij} = M_{ijkl} \hat{\sigma}_{kl} \tag{18}$$

with instantaneous compliances

$$M_{ijkl} = \frac{1+\nu}{2E} (\delta_{ik}\delta_{jl} + \delta_{il}\delta_{jk}) - \frac{\nu}{E} \delta_{ij}\delta_{kl} + \frac{1}{h} P_{ij} P_{kl}.$$

The inverse is

$$\hat{\sigma}_{ij} = L_{ijkl} D_{kl} \tag{19}$$

with instantaneous moduli

$$L_{ijkl} = L_{ijkl}^e - \frac{L_{ijmn}^e P_{mn} P_{rs} L_{rskl}^e}{h + P_{rs} L_{rsmn}^e P_{mn}}$$

where the elastic moduli are

$$L^e_{ijkl} = \frac{E}{1+\nu}\left[\frac{1}{2}(\delta_{ik}\delta_{jl} + \delta_{il}\delta_{jk}) + \frac{\nu}{1-2\nu}\delta_{ij}\delta_{kl}\right].$$

Plastic loading has been assumed in writing both (18) and (19); if the increment is elastic, only the elastic moduli and compliances are used. The effective plastic strain-rate is defined in terms of the logarithmic strain rates in the usual way as

$$\dot{\varepsilon}^P_e = \sqrt{2D^P_{ij}D^P_{ij}/3}. \tag{20}$$

4. Stress–strain behavior and calibration in shear

The influence of the modified version of the constitutive law is revealed by the stress–strain behavior in shear. Specifically, for a power law matrix material with $\sigma_M = \sigma_R(\varepsilon^P_M)^N$ and elasticity neglected ($E \to \infty$), stress–strain curves will be derived analytically for both pure shear and simple shear (Fig. 4) within a rigorous finite strain framework. Formulas for f and the strain associated with the maximum of shear stress will also be obtained. The maximum coincides with the onset of localization when there is a uniform distribution of void damage. The formulas are useful for calibrating the parameters of the model.

4.1. Pure shear

Consider pure shear in Fig. 4 with elastic strains neglected ($E \to \infty$). With $\sigma_I = \sigma_1 = \tau$ and $\sigma_{III} = \sigma_3 = -\tau\,(\tau > 0)$ as the only non-zero (true) stresses, $s_{ij} = \sigma_{ij}$, $\sigma_e = \sqrt{3}\tau$ and, from the yield condition, (6),

$$\sqrt{3}\tau = \sigma_M W(f) \quad \text{with } W(f) \equiv \sqrt{1 - 2q_1 f + q_3 f^2}. \tag{21}$$

By (7), $D^P_{33} = -D^P_{11}$ are the only non-zero strain rates with $D^P_{kk} = 0$, and, by (20), $\dot{\varepsilon}^P_e = 2D^P_{11}/\sqrt{3}$. Then, since D^P_{11} is the logarithmic strain rate, $\dot{\varepsilon}^P_1$, it follows that $\varepsilon^P_e = 2\varepsilon^P_1/\sqrt{3}$ where ε^P_1 is the logarithmic plastic strain component in the 1-direction. By (10), $\dot{f} = k_\omega f\dot{\varepsilon}^P_e$. With f_0 as the initial void volume fraction, it follows that

$$f/f_0 = e^{k_\omega \varepsilon^P_e}. \tag{22}$$

For the power law matrix it follows from (17) that $\dot{\sigma}_M = \sqrt{3}\tau N(\sigma_M/\sigma_R)^{-1/N}\dot{\varepsilon}^P_e/(1-f)$, which, in turn, can be integrated using (21) and $\dot{f} = k_\omega f\dot{\varepsilon}^P_e$ to give

$$\left(\frac{\sigma_M}{\sigma_R}\right)^{1/N} = \int_{f_0}^{f} \frac{W(\zeta)}{k_\omega\zeta(1-\zeta)}\,d\zeta \quad \text{and} \quad \frac{\sqrt{3}\tau}{\sigma_R} = W(f)\left[\int_{f_0}^{f} \frac{W(\zeta)}{k_\omega\zeta(1-\zeta)}\,d\zeta\right]^N. \tag{23}$$

Eqs. (22) and (23) provide an explicit recipe for generating τ as a function of ε^P_e. A set of illustrative curves is given in Fig. 5.
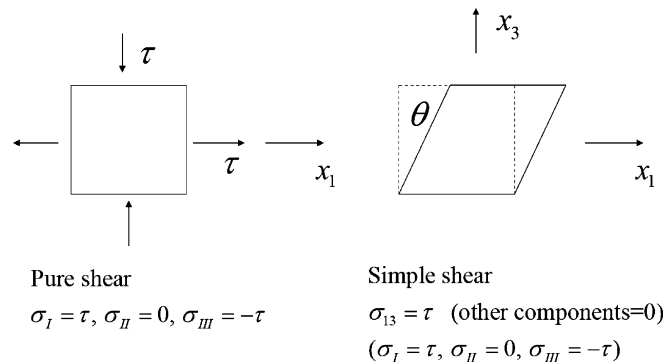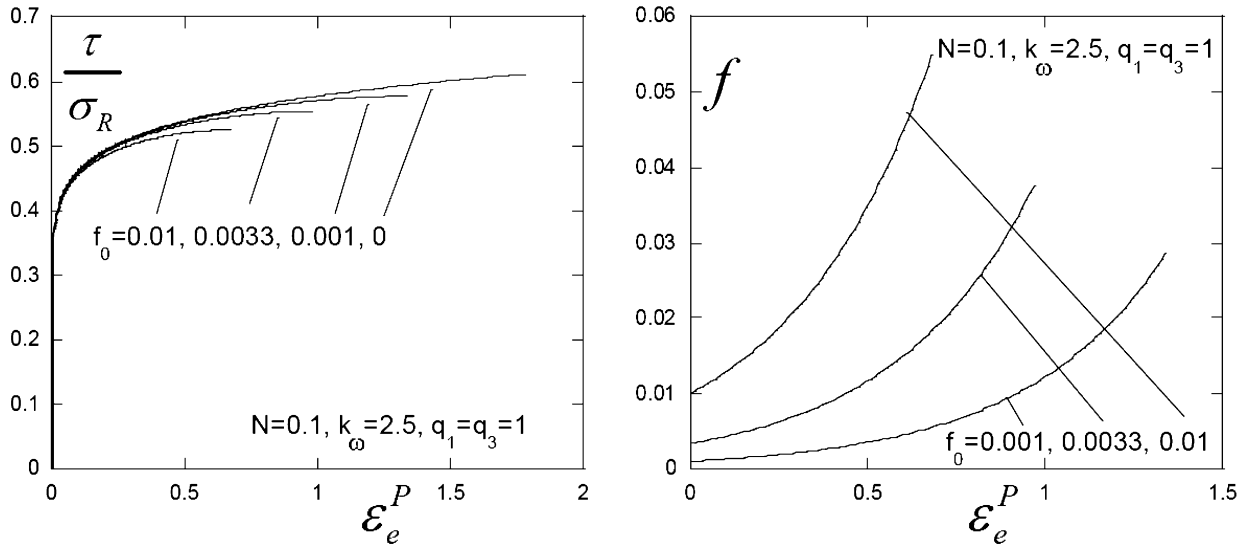

Fig. 4. Simple and pure shear.

Fig. 5. Shear stress τ and void volume fraction f as a function of effective plastic strain ε_e^p for pure or simple shear for various values of initial void volume fraction f_0.
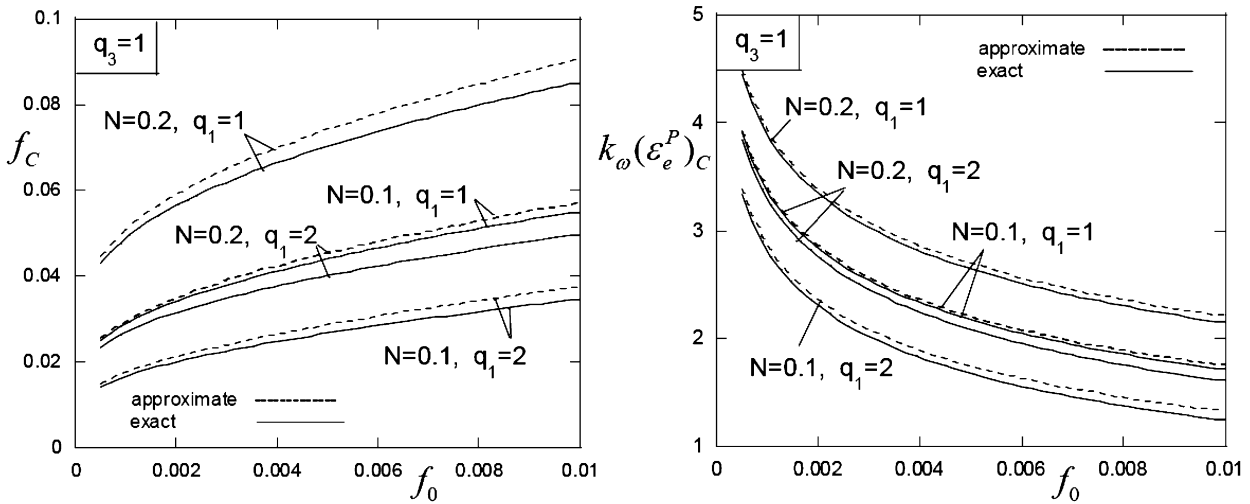

Fig. 6. Critical void volume fraction and effective plastic strain at shear band localization as a function of initial void volume fraction f_0 in pure and simple shear.

A further step yields equations for f_C and $(\varepsilon_e^P)_C$ associated with the maximum of τ at $d\tau/d\varepsilon_e^P = 0$:

$$\frac{NW(f_C)^3}{f_C(1 - f_C)} = (q_1 - q_3 f_C) \int_{f_0}^{f_C} \frac{W(\zeta)}{\zeta(1 - \zeta)} \, d\zeta \quad \text{and} \quad (\varepsilon_e^P)_C = \frac{1}{k_\omega} \ln\left(\frac{f_C}{f_0}\right). \tag{24}$$

Observe that f_C does not depend on k_ω, while the associated plastic strain is inversely proportional to k_ω. An accurate approximation to (24₁) can be obtained by anticipating that both f_0 and f_C are small and neglecting them compared to unity:

$$\frac{f_C}{f_0} \ln\left(\frac{f_C}{f_0}\right) \cong \frac{N}{q_1 f_0}. \tag{25}$$

Plots of f_C from both (24) and (25) with $k_\omega(\varepsilon_e^P)_C = \ln(f_C/f_0)$ are displayed in Fig. 6. The accuracy of the simple approximation (25) is evident revealing that N and q_1 appear as the ratio N/q_1. The other fitting parameter, q_3, has only a minor influence on these results, as suggested by (25).

4.2. Simple shear

The above results apply exactly to simple shear (Fig. 4) when elasticity is neglected. The detailed analysis, which requires use of the co-rotational stress rates and other relations introduced in the next section, is omitted and only the main result is reported. When elasticity is neglected, the only non-zero stress component is $\sigma_{13} = \tau$ in the fixed Cartesian axes and the only non-zero strain-rate component is $D_{13}^P = \dot{\theta}/(2\cos^2\theta)$. The effective strain rate (19) is $\dot{\varepsilon}_e^P = \dot{\theta}/(\sqrt{3}\cos^2\theta)$ for $\dot{\theta} > 0$ and, consequently,

$$\varepsilon_e^P = \frac{1}{\sqrt{3}}\tan\theta \quad \text{for } \theta > 0. \tag{26}$$

With ε_e^P defined above, (22) for f still applies as do (23), (24) and the approximation (25). Thus, Figs. 5 and 6 apply to simple shear as well as pure shear.

4.3. Calibration of k_ω from shear data

In pure or simple shear of a block of material with a uniform distribution of f_0, shear localization starts when the effective plastic strain reaches $(\varepsilon_e^P)_C$. Beyond this point, strain localizes in a shear band with unloading outside the band. Thus, $(\varepsilon_e^P)_C$ is an estimate of the overall effective plastic strain at fracture. Assume the initial void volume fraction, f_0, has already been identified using data from another test (e.g. an axisymmetric test or a mode I fracture test), and q_1, q_2 and q_3 have been chosen. In addition, assume the overall effective plastic strain associated with shear localization (or fracture) in pure or simple shear is known from an experiment and identify it as $(\varepsilon_e^P)_C$. Then, for a power law matrix material, the plot of $k_\omega(\varepsilon_e^P)_C$ in Fig. 6 or, alternatively Eqs. (24) can be used to determine k_ω. It is worth noting that the fitting parameter, q_1, which has been proposed based on solutions for voids subject to axisymmetric stress states (Tvergaard 1981, 1982), influences k_ω in this calibration process. Consequently, q_1 should not be altered once k_ω has been determined.

If the stress–strain curve, $\sigma_M(\varepsilon_M^P)$, characterizing the matrix material is not a power law, the calibration process is similar but elementary numerical work is needed to identify the maximum of the relation between τ and ε_e^P in shear. Eqs. (21) and (22) are still applicable, but (15) and (17) have to be used to obtain σ_M in terms of ε_e^P. Iteration on k_ω is required such that $(\varepsilon_e^P)_C$ coincides with the experimental value of the overall effective plastic at shear fracture.

5. Localization analysis

A study is performed to demonstrate the sensitivity of localization of plastic flow to the newly introduced constitutive parameter k_ω. An important objective is exploration of the relationship of the fracture strain, identified with the overall strain at localization, to stress triaxiality and the third invariant of stress as measured by ω or L. The problem analyzed is an infinite block of uniform material with initial damage, f_0^o, containing a thin, uniform planar band of material with larger initial damage, f_0^b. The material outside the band is subject to overall straining parallel to principal stress axes. The overall strain corresponding to localization of deformation within the band is determined, and the critical strain is computed as the minimum localization strain over all possible band orientations. The approach is a rigorous finite strain analysis that follows earlier localization studies first employed by Marciniak and Kuczynski (1967) to study localization in thin sheets under plane stress and laid out within a three-dimensional, finite strain setting by Rice (1977). This approach has been employed by several authors including Saje et al. (1982), Pan et al. (1983), and Mear and Hutchinson (1985). The following development closely follows Rice's (1977) treatment as detailed by Mear and Hutchinson (1985). The formulation requires consideration of only two states, those inside and outside the band, as the material in each region is initially uniform but with differing initial damage states.

Let the Cartesian axes (x_1, x_2, x_3) be the principal stress axes for the deformation history outside the band with $\sigma_I \equiv \sigma_1 \geqslant \sigma_{II} \equiv \sigma_2 \geqslant \sigma_{III} \equiv \sigma_3$, conforming with the conventions introduced earlier (see sketch in Fig. 7(a)). Outside the band, no rotation occurs and true stress increments are prescribed to satisfy

$$\dot{\sigma}_2 = R\dot{\sigma}_1 \quad \text{and} \quad \dot{\sigma}_3 = Q\dot{\sigma}_1 \tag{27}$$

where $Q \leqslant R \leqslant 1$. Except for plane strain deformations, R and Q are constant during each deformation history with σ_1 increased monotonically until the onset of localization. For plane strain deformations, which are not specifically considered here, Q is held constant and the condition $D_{22} = 0$ provides the evolution of R in terms of Q.
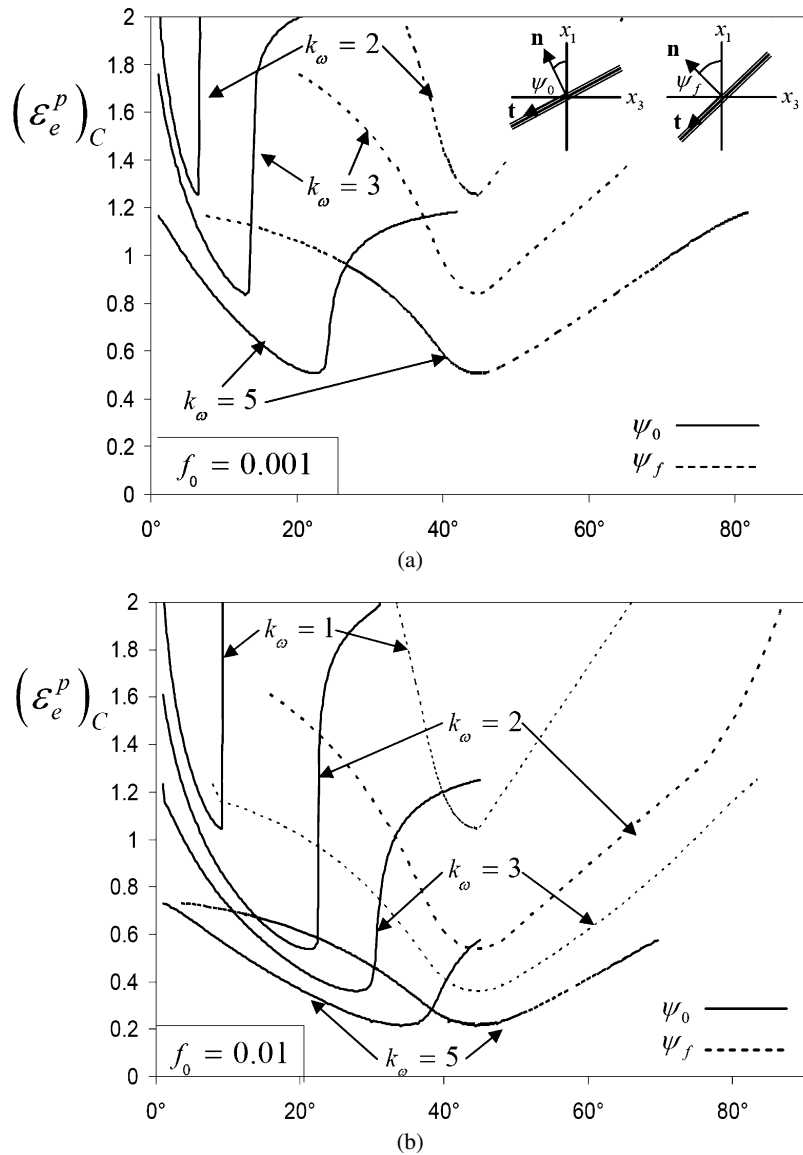
Fig. 7. Effective plastic strain $(\varepsilon_e^p)_C$ at localization under pure shear loading as a function of initial band angle, ψ_0, and angle at localization, ψ_f, for initial void fraction $f_0 = 0.001$ (a) and $f_0 = 0.01$ (b). Material parameters are $E = 200$ GPa, $\nu = 0.3$, $\sigma_Y = 200$ MPa, $N = 0.1$ and $q_1 = q_2 = q_3 = 1$.

Given the ordering of the applied principal stresses, the unit vector, $\mathbf{n}$, normal to the critical localization band can always taken to be perpendicular to the x_2 axis. Moreover, the direction of the tangential velocity discontinuity across the band, $\mathbf{t}$, will then also be perpendicular to the x_2 axis. In axisymmetric stressing, the critical band can be either normal or inclined to the x_1 axis. When inclined, the critical band orientation is not unique since all bands with that same inclination to the axis of symmetry are equally critical. Nevertheless, the unit normal may be taken to be normal to the x_2 axis in the analysis of the critical localization strain. Let ψ_0 be the angle between $\mathbf{n}$ and the x_1 axis in the undeformed state, and let ψ be that angle in the current state. These angles are related by

$$\tan \psi = e^{\varepsilon_1 - \varepsilon_3} \tan \psi_0 \tag{28}$$

where ε_1 and ε_3 are the logarithmic strains outside the band. In the current state,

$$\mathbf{n} = (\cos \psi, 0, -\sin \psi) \quad \text{and} \quad \mathbf{t} = (\sin \psi, 0, \cos \psi). \tag{29}$$

The velocity gradients, $v_{i,j}$, strain rates, D_{ij}, true stresses, σ_{ij}, and various stress rates are piecewise constant inside and outside the band. Denote quantities outside the band with a superscript o and quantities inside the band by the

superscript b. Continuity of velocities across the two interfaces between the planar band and the outside regions requires

$$v_{i,j}^b - v_{i,j}^o = \dot{d}_1 t_i n_j + \dot{d}_2 n_i n_j. \tag{30}$$

With H as the current thickness of the band, $\dot{d}_1 H$ is the tangential velocity jump across the band and $\dot{d}_2 H$ is the normal separation rate of the two band interfaces. Shear localizations have $|\dot{d}_1| \gg |\dot{d}_2|$, while normal localizations have $|\dot{d}_2| \gg |\dot{d}_1|$, as in the case of a band orientated normal to the symmetry axis in axisymmetric stressing ($\dot{d}_1 = 0$).

Let N_{ij} be the Cartesian components of the unsymmetrical nominal stress tensor (1st Piola–Kirchoff stress). Continuity of normal and tangential traction rates across the band requires

$$\left(\dot{N}_{ij}^b - \dot{N}_{ij}^o\right) n_i n_j = 0, \tag{31}$$

$$\left(\dot{N}_{ij}^b - \dot{N}_{ij}^o\right) n_i t_j = 0. \tag{32}$$

The nominal stress rate is related the to the Cartesian components of the Jaumann rate by

$$\dot{N}_{ij} = \hat{\sigma}_{ij} - \sigma_{jk} D_{ki} + \sigma_{ik} W_{jk} + \sigma_{ij} D_{kk} \tag{33}$$

where $W_{ij} = (v_{i,j} - v_{j,i})/2$. By the constitutive relation (19), the nominal stress rate may be expressed in terms of the velocity gradients as

$$\dot{N}_{ij} = c_{ijkl} v_{l,k} \tag{34}$$

where

$$c_{ijkl} = L_{ijkl} + \frac{1}{2}\sigma_{ik}\delta_{jl} - \frac{1}{2}\sigma_{il}\delta_{kj} - \frac{1}{2}\sigma_{jl}\delta_{ik} - \frac{1}{2}\sigma_{jk}\delta_{il} + \sigma_{ij}\delta_{kl}.$$

Inserting (30) into the equations for continuity of traction rates, (31) and (32), one obtains the following linear system of equations for $\dot{d}_1$ and $\dot{d}_2$:

$$c_{ijkl}^b \begin{bmatrix} n_i n_j n_k t_l & n_i n_j n_k n_l \\ n_i t_j n_k t_l & n_i t_j n_k n_l \end{bmatrix} \left\{ \begin{array}{c} \dot{d}_1 \\ \dot{d}_2 \end{array} \right\} = (c_{ijkl}^o - c_{ijkl}^b) v_{l,k}^o \left\{ \begin{array}{c} n_i n_j \\ n_i t_j \end{array} \right\}. \tag{35}$$

An incremental solution is accomplished by prescribing $v_{l,k}^o$ in each step consistent with small prescribed increments of a quantity such as the maximum principal stress or strain outside the band. In matrix form, (35) is $\mathbf{A}\dot{\mathbf{d}} = \dot{\mathbf{b}}$. Thus, given the current band orientation, an imposed velocity gradient on the material outside the band, and the current states inside and outside the band, a solution for $\dot{d}_1$ and $\dot{d}_2$ can be found unless $\det(\mathbf{A}) = 0$, which corresponds to the localization condition. Supplementing (35) is the equation for computing the stress increments:

$$\dot{\sigma}_{ij} = \hat{\sigma}_{ij} - \sigma_{ik} W_{kj} + \sigma_{jk} W_{ik} \tag{36}$$

with all components being Cartesian with respect to the x_i axes.

For stress increments constrained by (27), the non-zero velocity gradients outside the band can be expressed in terms of $v_{1,1}^o$ by

$$v_{2,2}^o = \frac{c_{2233}^o c_{3311}^o + R(c_{3333}^o c_{1111}^o - c_{1133}^o c_{3311}^o) + Q(c_{1133}^o c_{2211}^o - c_{2233}^o c_{1111}^o) - c_{3333}^o c_{2211}^o}{c_{3333}^o c_{2222}^o + R(c_{3322}^o c_{1133}^o - c_{3333}^o c_{1122}^o) + Q(c_{1122}^o c_{2233}^o - c_{1133}^o c_{2222}^o) - c_{3322}^o c_{2233}^o} v_{1,1}^o,$$

$$v_{3,3}^o = \frac{c_{3322}^o c_{2211}^o + R(c_{1122}^o c_{3311}^o - c_{3322}^o c_{1111}^o) + Q(c_{2222}^o c_{1111}^o - c_{1122}^o c_{2211}^o) - c_{2222}^o c_{3311}^o}{c_{3322}^o c_{2233}^o + R(c_{3333}^o c_{1122}^o - c_{3322}^o c_{1133}^o) + Q(c_{1133}^o c_{2222}^o - c_{1122}^o c_{2233}^o) - c_{3333}^o c_{2222}^o} v_{1,1}^o \tag{37}$$

such that $D_{11}^o = v_{1,1}^o$ can be prescribed prior to localization. For problems with plane strain conditions outside the band ($D_{22} = v_{2,2}^o = 0$), (37) provides an equation relating R to prescribed Q.

6. Localization predictions

For the numerical results presented below, the relation between the true stress and logarithmic strain for the matrix material (i.e. the material with $f = 0$) is taken as

$$\frac{\varepsilon}{\varepsilon_Y} = \begin{cases} \sigma/\sigma_Y, & \sigma \leqslant \sigma_Y, \\ (\sigma/\sigma_Y)^{1/N}, & \sigma > \sigma_Y \end{cases} \tag{38}$$
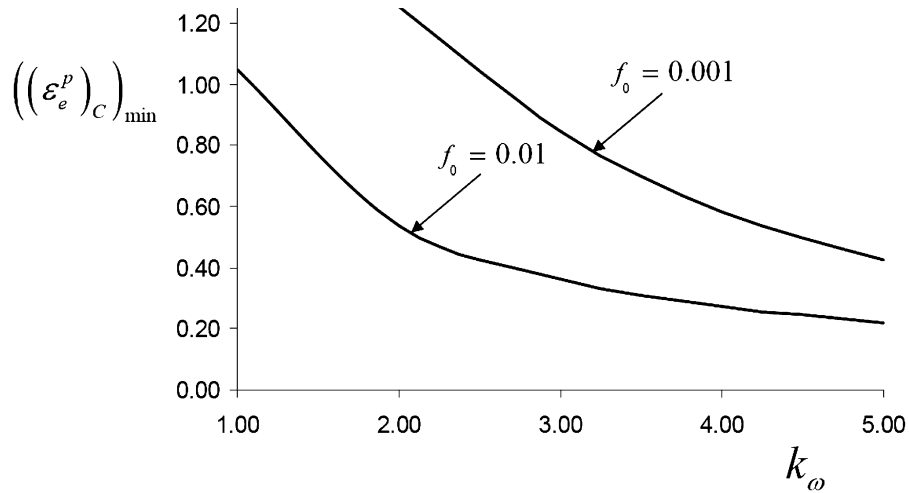
Fig. 8. Minimum effective plastic strain $((\varepsilon_e^P)_C)_{min}$ at localization over all band orientations under pure shear loading as a function of k_ω for $f_0 = 0.001$ and $f_0 = 0.01$. Material parameters are $E = 200$ GPa, $\nu = 0.3$, $\sigma_Y = 200$ MPa, $N = 0.1$ and $q_1 = q_2 = q_3 = 1$.

where $\sigma_Y = E\varepsilon_Y$. In all the numerical examples, $E = 200$ GPa, $\nu = 0.3$, $\sigma_Y = 200$ MPa, $N = 0.1$ and $q_1 = q_2 = q_3 = 1$; void nucleation is not included.

6.1. Localization in pure shear—the influence of k_ω

Consider the plane stress state of pure shear with $R = 0$ and $Q = -1$ in (27), i.e. $\sigma_3 = -\sigma_1$ and $\sigma_2 = 0$. The effective plastic strain outside the band at localization, $(\varepsilon_e^P)_C$, is plotted as a function of the initial orientation of the imperfection band, ψ_0, and the orientation at localization, ψ_f, for $f_0^b = 0.001$ in Fig. 7(a) and for $f_0^b = 0.01$ in Fig. 7(b). Predictions for various values of k_ω are shown. In these cases, the void volume fraction outside the band, f_0^o, is zero. No localization occurs in this case for the unmodified Gurson model with $k_\omega = 0$.

It is evident in Fig. 7 that the orientation of the imperfection band giving rise to the minimum localization strain is nearly 45° *in the state when localization occurs*. Accordingly, the initial orientation associated with the minimum is a strong function of the strain to localization. Plots of the minimum localization strain over all possible orientations, $((\varepsilon_e^P)_C)_{min}$, are given in Fig. 8 for two levels of initial void volume fraction in the band. As with the calibration curves in Fig. 6, these results can be used to gauge the value of k_ω required to produce a specific level of fracture strain in pure shear.

6.2. Influence of initial void volume fraction outside the band

The effect of voids outside the band is displayed in Fig. 9, again for pure shear with $R = 0$ and $Q = -1$. In this plot, the initial void volume fraction inside the band is fixed at $f_0^b = 0.01$ while the initial volume fraction outside the band is varied over the range $0 \leqslant f_0^o/f_0^b \leqslant 1$. The lowest critical strain corresponds to the largest non-uniformity with no voids outside the band, as in the cases plotted in Figs. 7 and 8. In the limit when the initial void distribution is uniform $(f_0^o/f_0^b = 1)$, localization occurs as a bifurcation. While there is some sensitivity to the initial non-uniformity, it is of secondary importance compared to the magnitude of initial void volume fraction in the band, f_0^b. In the examples that follow, we will continue to take $f_0^o = 0$.

6.3. The roles of $\omega(\sigma)$ and σ_m/σ_e in localization and fracture

With reference to Fig. 3, note again that axisymmetric stress states outside the band are either uniaxial tension plus a hydrostatic component ($\sigma_I > \sigma_{II} = \sigma_{III}$) with $\omega = 0$ and $L = -1$ or equi-biaxial tension plus a hydrostatic component ($\sigma_I = \sigma_{II} > \sigma_{III}$) with $\omega = 0$ and $L = 1$. States outside the band comprised of a pure shear stress plus a hydrostatic component ($\sigma_I = \tau + \sigma_m$, $\sigma_{II} = -\tau + \sigma_m$, $\sigma_{III} = \sigma_m$ with $\tau > 0$) have $\omega = 1$ and $L = 0$.

Curves of the minimum plastic strain at localization versus triaxiality for specified values of ω in Figs. 10–12 bring out the significant role of k_ω in the modified version of the constitutive model, especially in the range of low
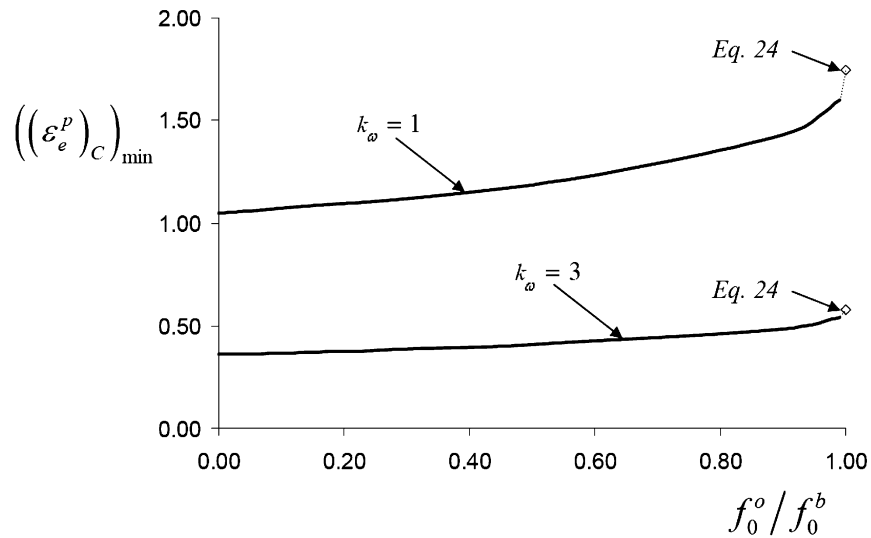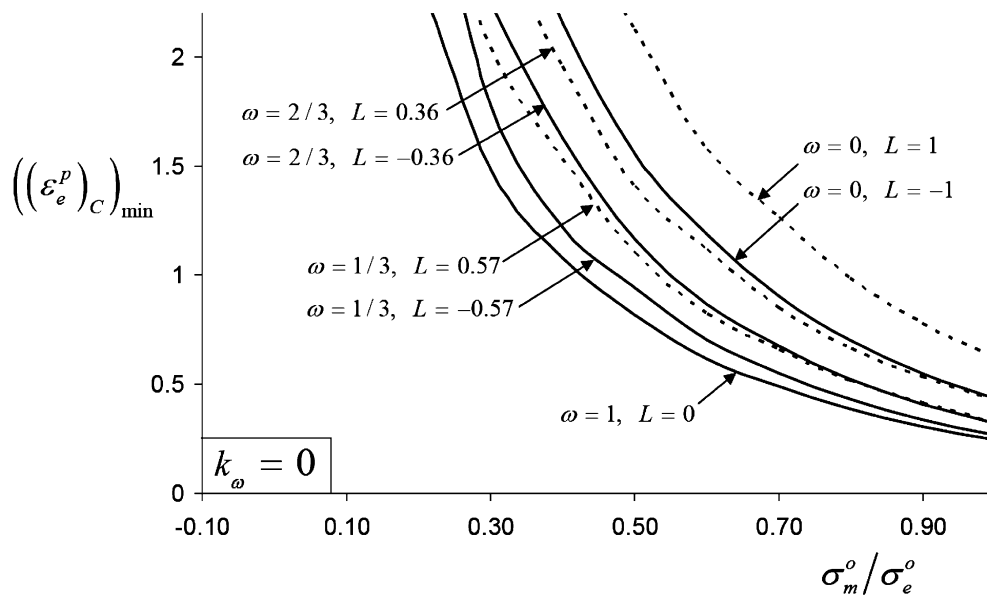
Fig. 9. Minimum effective plastic strain $((\varepsilon_e^p)_C)_{min}$ at localization over all band orientations under pure shear loading as a function of the ratio of initial void volume fractions outside, f_0^o, and inside, f_0^b, the band for $k_\omega = 1$ and $k_\omega = 3$. The initial void volume fraction inside the band is fixed as $f_0^b = 0.01$. Localization in the limit $f_0^o/f_0^b \to 1$ occurs as a bifurcation. Material parameters are $E = 200$ GPa, $v = 0.3$, $\sigma_Y = 200$ MPa, $N = 0.1$ and $q_1 = q_2 = q_3 = 1$.

Fig. 10. Minimum effective plastic strain $((\varepsilon_e^p)_C)_{min}$ at localization over all band orientations for constant values of ω as predicted by the un-modified Gurson Model ($k_\omega = 0$). Material parameters are $E = 200$ GPa, $v = 0.3$, $\sigma_Y = 200$ MPa, $N = 0.1$, $q_1 = q_2 = q_3 = 1$, $f_0^b = 0.01$ and $f_0^o = 0$.

triaxiality. In these figures, ω and L are associated with the overall stress state, i.e. the stress state outside the band. Of primary relevance to the present investigation, is the fact that the results based on the unmodified Gurson Model ($k_\omega = 0$) predict that localization is effectively excluded for any stress state at triaxialities below about 0.3. While stress states corresponding to a pure shear stress plus hydrostatic tension ($\omega = 1$ and $L = 0$) are more susceptible to localization than axisymmetric states at the same triaxiality, the spread over the entire range of ω or L is not nearly as large as seen in some of the sets of experimental data. For the modified model, the significant role of the second measure of stress state is seen in Fig. 11 for $k_\omega = 1$ and Fig. 12 for $k_\omega = 3$. For axisymmetric stress states, k_ω has very little influence on localization as can be seen by comparing the curves for $L = \pm 1$ in Figs. 11 and 12 those in Fig. 10 for the unmodified Gurson Model. While the effect of k_ω is strictly absence on behavior outside the band for these states, it has a small effect on behavior inside the band and, thus on the localization strain, because the orientation
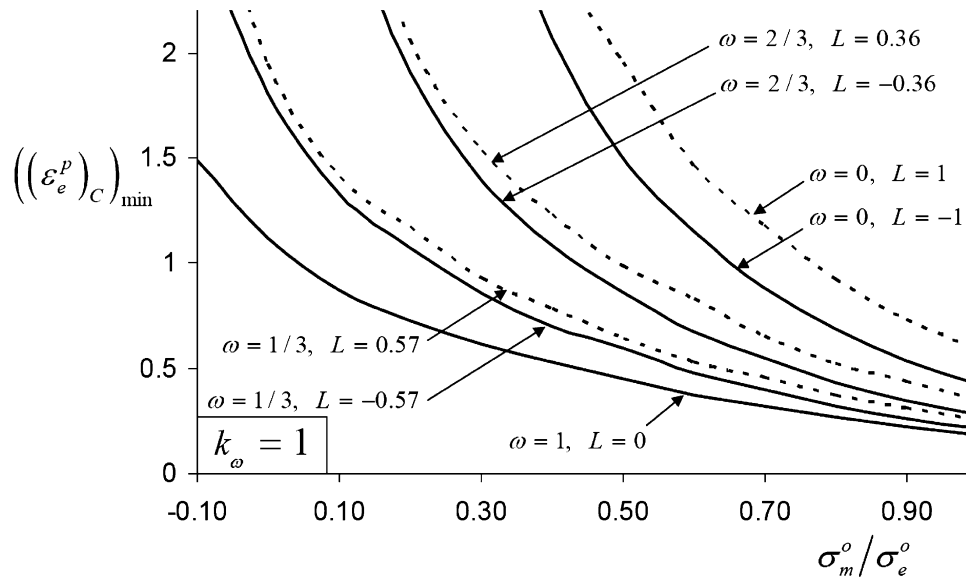
K. Nahshon, J.W. Hutchinson / European Journal of Mechanics A/Solids 27 (2008) 1–17

Fig. 11. Minimum effective plastic strain $((\varepsilon_e^p)_C)_{\min}$ at localization over all band orientations for constant values of ω as predicted by the modified Gurson Model for $k_\omega = 1$. Material parameters are $E = 200$ GPa, $\nu = 0.3$, $\sigma_Y = 200$ MPa, $N = 0.1$, $q_1 = q_2 = q_3 = 1$, $f_0^b = 0.01$ and $f_0^o = 0$.
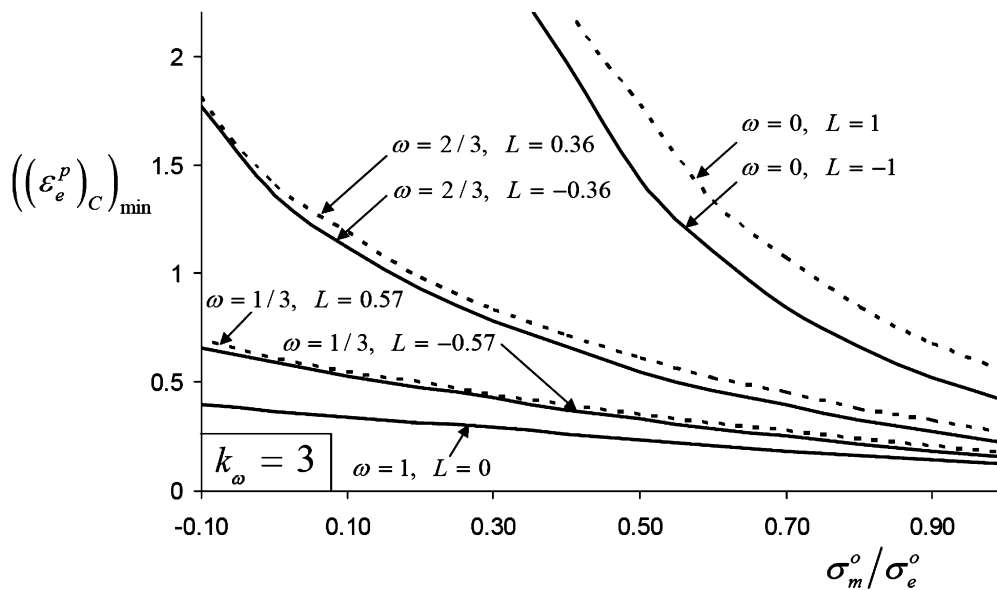
Fig. 12. Minimum effective plastic strain $((\varepsilon_e^p)_C)_{\min}$ at localization over all band orientations for constant values of ω as predicted by the modified Gurson Model for $k_\omega = 3$. Material parameters are $E = 200$ GPa, $\nu = 0.3$, $\sigma_Y = 200$ MPa, $N = 0.1$, $q_1 = q_2 = q_3 = 1$, $f_0^b = 0.01$ and $f_0^o = 0$.

of the band associated with the minimum localization strain is not precisely normal to the maximum principal stress direction. Thus, material within the band develops a small component of shear.

The modification introduced in this paper highlights the difference between shear and axisymmetric states, leaving behavior for axisymmetric stressing unaltered. By choosing $\omega(\sigma)$ as the second measure of the stress state, we have ignored any role of the sign of L on the constitutive behavior and, specifically, our modification makes no attempt to distinguish between the two types of axisymmetric stress states with $L = -1$ and $L = 1$. This decision was based our desire to introduce a modification having as few additional parameters as possible, coupled to the fact that we are unaware of experimental data for fracture or localization strains that would allow us to discriminate between states with $L = -1$ and $L = 1$. If subsequent experimental data for states with $L = 1$ suggest that there is an important difference in localization and fracture strains from those with $L = -1$, the present modification can be extended to capture the effect. A modification of the Gurson Model employing the Lode parameter has been pursued by Xue (2007a, 2007b). Further numerical simulations of void growth and coalescence along the lines conducted by Barsoum
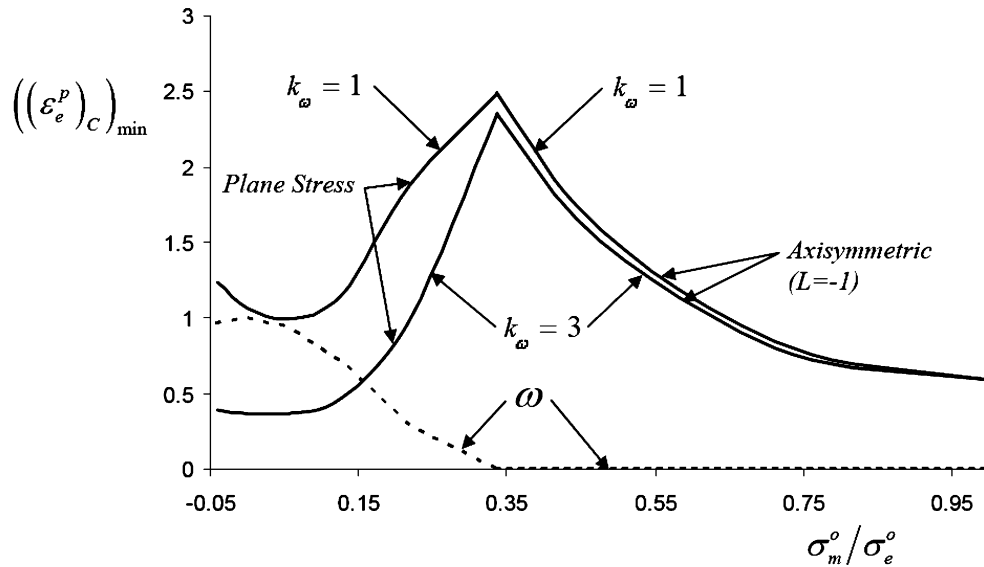
Fig. 13. Minimum effective plastic strain $((\varepsilon_e^p)_C)_{\min}$ at localization over all band orientations as a function of stress triaxiality outside the band under axisymmetric ($\sigma_m^o/\sigma_e^o \geqslant 1/3$) and plane stress conditions ($\sigma_m^o/\sigma_e^o \leqslant 1/3$) for $k_\omega = 1$ and $k_\omega = 3$. Additionally, the parameter ω associated with the state outside the band is shown. Material parameters are $E = 200$ GPa, $\nu = 0.3$, $\sigma_Y = 200$ MPa, $N = 0.1$, $q_1 = q_2 = q_3 = 1$, $f_0^b = 0.01$ and $f_0^o = 0$.

and Faleskog (2007b) and Gao and Kim (2006) can be used to gain important insights into dependence on the Lode parameter.

The role of ω, and, thus, of L, on the localization strains in Figs. 11 and 12 is dramatic, but not out of line with the limited experimental data taken for both axisymmetric and non-axisymmetric states in the literature (e.g. Bao and Wierzbicki, 2004; Barsoum and Faleskog, 2007a; Johnson and Cook, 1985). The present modification of the Gurson Model introduces one new material parameter, k_ω, which is most readily assigned by calibration against data for localization or fracture in shear, as discussed in some detail in Section 4. Based on the limited data in the literature, it would appear that k_ω should lie in the range $1 < k_\omega < 3$ for many structural alloys.

6.4. An illustration of the importance of the stress state measures $\omega(\boldsymbol{\sigma})$ and σ_m/σ_e

Most of the fracture strain data in Fig. 1 from Bao and Wierzbicki (2004) for Al 2024-T351 aluminum was obtained using two distinct types of specimens. Fracture strains from tensile tests of notched round bar specimens are associated with *axisymmetric stress states* ($R = Q < 1$ with $\omega = 0$ and $L = -1$). The low triaxiality data is obtained from upsetting tests obtained by compressing stubby cylindrical specimens that are constrained at their ends. For these specimens, localization and shear cracking occur at the surface under *states of plane stress* ($R = 0$, $Q \leqslant 0$, with $\omega \geqslant 0$). Fig. 13 plots minimum effective plastic at localization as a function of triaxiality, σ_m/σ_e, for the two types of stress states for $k_\omega = 1$ and 3 with $f_0^b = 0.01$ and $f_0^o = 0$. Included in this figure is a plot of ω associated with the stress state outside the band. Under axisymmetric stressing for $\sigma_m/\sigma_e < 1/3$, localization occurs at very large strains, and the curve in Fig. 13 has been terminated at $\sigma_m/\sigma_e = 1/3$ corresponding to uniaxial tension. Note, again, that k_ω has very little effect on localization under applied axisymmetric stress states. As seen in Fig. 13, the modified Gurson Model predicts a very strong dependence of the localization strain on whether the applied stress state is plane stress or axisymmetric, in accord with the trends in the Bao and Wierzbicki (2004) data in Fig. 1. No attempt has been made to fit the data in Fig. 1. However, it is clear from Fig. 13 that f_0^b and k_ω can be chosen such that the predictions will quantitatively capture data trends. The state of pure shear in plane stress has $\sigma_m/\sigma_e = 0$. Localization is even predicted under slightly negative triaxiality for plane stress states. The cusp-like behavior seen in the original Bao and Wierzbicki (2004) data plot is associated with intersection of the plane stress branch of the data with the axisymmetric branch at the state of uniaxial tension at $\sigma_m/\sigma_e = 1/3$, as seen in Fig. 13. Similar trends emerge from a damage model introduced by Xue (2007a, 2007b) which ties damage development to both triaxiality and the Lode parameter.

7. Concluding remarks

The modification of the Gurson Model introduced here incorporates a contribution to ductile damage growth under shear-dominated stress states in a way that leaves behavior under axisymmetric stress states unaltered. One new parameter, k_ω, is introduced which sets the rate of damage development in shear. The modified model is capable of modeling localization and fracture in shear-dominated stress states with low triaxiality. The model captures experimental trends recently reported for various structural alloys displaying a marked difference between fracture strains under axisymmetric stressing from those under a pure shear stress plus a hydrostatic component or under plane stress states.

Calibration of the new parameter for a specific material is proposed based on experimental data on shear localization or fracture. The modified model has been implemented as a user-material constitutive subroutine in ABAQUS/Explicit (Nahshon and Xue, 2007). This code is currently being used to study several basic problems in which the issues addressed in this paper are crucial, including a shear-off experiment designed to measure fracture behavior in shear and the transition from ductile necking failure to shear-off failure in clamped plates subject to intense blast loads.

Acknowledgements

References

Anderson, P.M., Fleck, N.A., Johnson, K.L., 1990. Localization of plastic deformation in shear due to microcracks. J. Mech. Phys. Solids 38, 681–699.

Bao, Y., Wierzbicki, T., 2004. On fracture locus in the equivalent strain and stress triaxiality space. Int. J. Mech. Sci. 46 (81), 81–98.

Barsoum, I., Faleskog, J., 2007a. Rupture in combined tension and shear: Experiments. Int. J. Solids Structures 44, 1768–1786.

Barsoum, I., Faleskog, J., 2007b, Rupture in combined tension and shear: Micromechanics, Int. J. Solids Structures, in press.

Chu, C.C., Needleman, A., 1980. Void nucleation effects in biaxially stretched sheets. J. Engrg. Mat. Tech. 102, 249–256.

Gao, X., Kim, J., 2006. Modeling of ductile fracture: Significance of void coalescence. Int. J. Solids Structures 43, 6277–6293.

Gologanu, M., Leblond, J.-B., Perrin, G., Devaux, J., 1995. Recent extensions of Gurson's model for porous ductile metals. In: Suquet, P. (Ed.), Continuum Micromechanics. Springer-Verlag.

Gullerud, A.S., Gao, X., Dodds, R.H., Haj-Ali, R., 2000. Simulation of ductile crack growth using computational cells: numerical aspects. Engrg. Fracture Mech. 66, 65–92.

Gurson, A.L., 1977. Continuum Theory of ductile rupture by void nucleation and growth – Part I. Yield criteria and flow rules for porous ductile media. J. Engrg. Mat. Tech. 99, 2–15.

Hancock, J.W., Mackenzie, A.C., 1976. On the mechanisms of ductile fracture in high-strength steels subject to multi-axial stress-states. J. Mech. Phys. Solids 24, 147–160.

Howard, I.C., Li, Z.H., Bilby, B.A., 1994. Ductile crack growth predictions for large center cracked panels by damage modeling using 3-D finite element analysis. Fatigue and Fracture Engrg. Mater. Struct. 17, 959–969.

Hutchinson, J.W., Pardoen, T., 2000. An extended model for void growth and coalescence. J. Mech. Phys. Solids 48, 2467–2512.

Johnson, G.R., Cook, W.H., 1985. Fracture characteristics of three metals subjected to various strains, strain rates, temperatures and pressures. Engrg. Fracture Mech. 21 (1), 31–48.

Leblond, J.-B., Perrin, G., Devaux, J., 1995. An improved Gurson-type model for hardenable ductile metals. Eur. J. Mech. A Solids 14, 499–527.

Le Roy, G., Embury, J.D., Edwards, G., Ashby, M.F., 1981. A model of ductile fracture based on the nucleation and growth of voids. Acta Met. 29, 1509–1522.

Marciniak, Z., Kuczynski, K., 1967. Limit strains in the processes of stretch-forming sheet metal. Int. J. Mech. Sci. 9 (9), 609–612.

Mear, M.E., Hutchinson, J.W., 1985. Influence of yield surface curvature on flow localization in dilatant plasticity. Mech. Mat. 4, 395–407.

McClintock, F.A., 1968. A criterion of ductile fracture by the growth of holes. J. Appl. Mech. 35, 363–371.

McClintock, F.A., 1971. Plasticity aspects of fracture. In: Leibowitz, H. (Ed.), Fracture, vol. 3. Academic Press, pp. 47–225.

Nahshon, K., Xue, Z., 2007. Numerical Implementation of a shear damage modified Gurson Model and its application to punch out experiments, in preparation.

Needleman, A., Rice, J.R., 1978. Limits to ductility set by plastic flow localization. In: Koistinen, D.P., et al. (Eds.), Mechanics of Sheet Metal Forming. Plenum Publishing, pp. 237–267.

Rice, J.R., 1977. The localization of plastic deformation. In: Koiter, W.T. (Ed.), Theoretical and Applied Mechanics, vol. 1. North-Holland Publishing, Delft, pp. 207–220.

Rice, J.R., Tracey, D.M., 1969. On the ductile enlargement of voids in triaxial stress fields. J. Mech. Phys. Solids 17, 201–217.

Rousselier, G., 1987. Ductile fracture models and their potential in local approach of fracture. Nuclear Engrg. Design 105, 97–111.

Saje, M., Pan, J., Needleman, A., 1982. Void nucleation effects on shear localization in porous plastic solids. Int. J. Fracture 19, 163–182.

Pan, J., Saje, M., Needleman, A., 1983. Localization of deformation in rate sensitive porous plastic solids. Int. J. Fracture 21, 261–278.

Teirlinck, D., Zok, F., Embury, J.D., Ashbt, M.F., 1988. Acta Met. 36 (5), 1213–1228.

Teng, X., Wierzbicki, T., 2006. Evaluation of six fracture models in high velocity perforation. Engrg. Fracture Mech. 73, 1653–1678.

Tvergaard, V., 1981. Influence of voids on shear band instabilities under plain strain conditions. Int. J. Fracture 17, 389–407.

Tvergaard, V., 1982. On localization in ductile materials containing spherical voids. Int. J. Fracture 18, 237–252.

Tvergaard, V., 1990. Material failure by void growth. Adv. Appl. Mech. 27, 83–151.

Weck, A., Wilkinson, D.S., Toda, H., Maire, E., 2006. 2D and 3D visualization of ductile fracture. Adv. Engrg. Mater. 8 (6), 469–472.

Xia, L., Shih, C.F., Hutchinson, J.W., 1995. A computational approach to ductile crack growth under large scale yielding conditions. J. Mech. Phys. Solids 43, 398–413.

Xue, L., 2007a. Ductile fracture modeling—theory, experimental investigation and numerical verification. Ph.D. thesis, Massachusetts Institute of Technology.

Xue, L., 2007b. Damage accumulation and fracture initiation in uncracked ductile solids subject to triaxial loading. Int. J. Solids Structures 44 (16), 5163–5181.